Commun. Comput. Phys.
doi: 10.4208/cicp.141009.241110s

Vol. **9**, No. 5, pp. 1284-1292
May 2011

# A New Boundary Condition for Three-Dimensional Lattice Boltzmann Simulations of Capillary Filling in Rough Micro-Channels

Alessandro De Maio[1,*], Silvia Palpacelli[1] and Sauro Succi[2,3]

[1] *Numidia s.r.l., via Berna 31, 00144 Roma, Italy.*
[2] *Istituto Applicazioni Calcolo, CNR, via dei Taurini 19, 00185 Roma, Italy.*
[3] *Freiburg Institute for Advanced Studies, School of Soft Matter Research, Albertstr. 19, 79104 Freiburg im Breisgau, Freiburg, Germany.*

Received 14 October 2009; Accepted (in revised version) 24 November 2010

Available online 18 February 2011

**Abstract.** A new boundary condition, aimed at inhibiting near-wall condensation effects in lattice Boltzmann simulations of capillary flows in micro-corrugated channels, is introduced. The new boundary condition is validated against analytical solutions for smooth channels and demonstrated for the case of three-dimensional microflows over randomly corrugated walls.

**PACS**: 47.11.-j, 47.55.Ca, 47.61.-k

**Key words**: Microfluidics, capillary flows, lattice Boltzmann simulation.

## 1 Introduction

The Lattice Boltzmann method was devised as a computational alternative to the solution of the Navier-Stokes equations for the numerical simulation of macroscopic flows [1]. For the last few years, however, an intense activity has been directed by many groups towards the application of LB techniques to microscopic and nanoscopic flows [2–7]. The somewhat unanticipated success of LB beyond the macroscopic context is probably due to the existence of a large body of microfluidic problems, in fact larger than textbook indications, for which continuum hydrodynamics is violated, but somehow mildly, i.e., in a way which can be mended without necessarily resorting to atomistic simulations (molecular dynamics). This statement can be made a little more precise as follows. The breakdown of hydrodynamics in microfluidic problems is often signalled by the appearance of infinities/singularities in the corresponding solutions. Moving contact lines, droplet

*Corresponding author. *Email addresses:* demaio.a@gmail.com (A. De Maio), silviapalpacelli@gmail.com (S. Palpacelli), succi@iac.rm.cnr.it (S. Succi)

 

break-up and coalescence, are just but a few examples in point [8–10]. It is generally understood that such infinities are regulated by an atomistic cutoff. Nevertheless, going all the way down to atomistic simulation proves unpractical for want of compute power. This no-fly zone offers in principle a rich hunting ground for mesoscopic/kinetic methods. However, achieving quantitative accuracy is by no means a given, and depends on a careful application of these methods in the appropriate parameter regime. In this paper we shall discuss a few aspects related to the specific case of capillary front-propagation in rough geometries.

## 2 The method

We use the LB method with the standard Shan-Chen (SC) [11] pseudo-potential forcing. The corresponding lattice Boltzmann equation takes the following form:

$$f_i(\vec{r}+\vec{c}_i\Delta t,t+\Delta t)-f_i(\vec{r},t)=\frac{\Delta t}{\tau}\left(f_i^{eq}(\vec{r},t)-f_i(\vec{r},t)\right), \tag{2.1}$$

where $f_i(\vec{r},t)$ represents the probability of finding a particle at time $t$ on the lattice site $\vec{r}$, moving with velocity $\vec{c}_i$. The left-hand-side represents the particle free-streaming, while the right hand side encodes particle collisions in the form of a relaxation on a time scale $\tau$ to the local equilibrium $f_i^{eq}$. The latter is given by a Maxwell-Boltzmann distribution truncated to second order in the local Mach number, and reads as follows:

$$f_i^{eq}(\vec{r},t)=\rho w_i\left(1+\frac{\vec{u'}\cdot\vec{c}_i}{c_s^2}+\frac{\vec{u'}\vec{u'}:\vec{\vec{Q}}_i}{2c_s^4}\right), \tag{2.2}$$

where $w_i$ are the standard weights for the 19-speed 3d lattice considered in this work, and $\vec{\vec{Q}}=\vec{c}_i\vec{c}_i-c_s^2 I$ is the quadrupole projector upon the i-the direction, $c_s^2=\sum_i w_i c_{ix}^2$, being the lattice sound speed. In the above, $\rho=\sum_i f_i$ is the local fluid density and $\vec{u'}=(\sum_i f_i\vec{c}_i+\vec{F}\tau)/\rho$ is the local fluid speed, including the contribution of the interparticle-interaction force

$$\vec{F}=-G\Psi(\vec{r};t)\sum_i w_i\Psi(\vec{r}+\vec{c}_i\Delta t)\vec{c}_i. \tag{2.3}$$

In the above, $G$ is the coupling strength, and $\Psi$ is the usual density-dependent pseudo-potential $\Psi(\rho)=(1-e^{-\rho})$. As is well known, the SC method provides the two basic features of non-ideal fluid behavior, namely a non-ideal equation of state $p=\rho c_s^2+Gc_s^2\Psi^2/2$, and a non-zero surface tension

$$\gamma\propto-\frac{G}{2}c_s^4\int(\nabla\Psi)^2dy,$$

where $y$ runs across the interface. It is readily shown that for $G<-4$, the above equation of state generates coexisting liquid and vapor phases.

The SC method also allows the definition of a contact angle at the triple contact point between the liquid/vapor interface and a solid wall. A practical way of modeling fluid-wall interactions is to set the value of the pseudo-potential at a wall site $W$ to a prescribed value, specified by a surface-density parameter $\rho_W$ [12] (not to be identified with the fluid density at the wall):

$$\Psi(W)=\Psi(\rho_W). \tag{2.4}$$

Increasing values of $\rho_W$ code for decreasing contact angles (the fluid is attracted to the wall), covering the full range $0^\circ-180^\circ$. A convenient alternative is to set the surface density through a given surplus/deficit with respect to the surrounding fluid, i.e.,

$$\Psi(W)\equiv\Psi(\rho_W)=\Psi(\bar{\rho}_F+\Delta), \tag{2.5}$$

where $\Delta$ is the density surplus and bar indicates a weighted average over the fluid sites $F$ connected to the wall site $W$. Essentially, this boundary condition keeps a fixed density gradient at the wall, and again, increasing values of $\Delta$ code for decreasing contact angle. In particular, for $G=-5$, the dependence between the contact angle $\theta$ and the parameter $\Delta$ is well fitted by the following linear relation:

$$\theta=90(1-1.83\Delta).$$

## 3 Boundary conditions with rough walls

Due to the limited liquid/vapor density ratios supported by the SC method, both boundary conditions are prone to spontaneous condensation, especially for vapor in deep valleys, i.e., light-fluid sites surrounded by a majority of wall sites (see Fig. 1). In fact, such sites experience enhanced wall-interaction, which eventually leads to condensation before the capillary front has time to reach the valley. As a result, the valley is literally hidden (filled up) by the condensed liquid, so that the front can proceed nearly like on a smooth surface, thereby suffering less mechanical friction than in the absence of condensation.

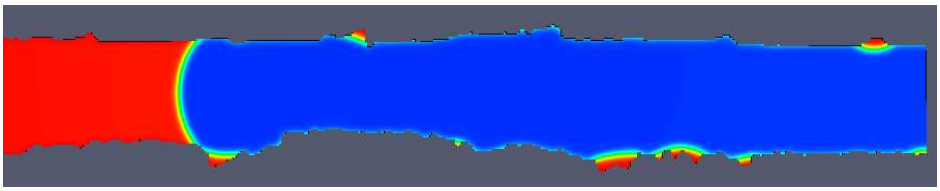

Figure 1: Spurious condensation of fluid sites surrounded by solid sites.

We wish to point out that the opposite situation, i.e., liquid suffering *less* friction upon sliding over a vapour/gas layer, sometimes referred to as "super-hydrophobicity", is ruled out on the basis of the size of our micro-corrugations, which is well above the nanometric scales usually required for the onset of super-hydrophobicity [13].

It should also be emphasized that local condensation effects in micro-cavities might well bear a physical relevance, for fluids sufficiently close to the critical point. Here, however, we wish to address situations well away from the critical point (such is typically the case for current experiments), so that local micro-condensation can essentially be ruled out on a thermodynamic basis. It is only in this respect that such condensation effects are referred to as "artificial/spurious" in the present work. As to the relatively low liquid/vapor density ratios attained in the simulations, it has been shown that above $\rho_L/\rho_V > 10$, the density ratio has negligible effects on the front propagation, so that condensation phenomena can safely be neglected [14, 15].

To prevent artificial fill-up, we have modified the boundary condition Eq. (2.5) as follows. The idea is to apply the density surplus only if the fluid density exceeds a given density threshold, i.e.,

$$\rho(W) = \bar{\rho}(F) + \Delta\,\mathcal{H}(\bar{\rho}(F) - K\rho_L), \tag{3.1}$$

where the Heaviside function, $\mathcal{H}$, implies that the density surplus applies only to the sites such that $\bar{\rho}(F) > K\rho_L$. Here, $K$ is an inhibition parameter and $\rho_L$ is the (initial) liquid density. This way, the wall is "passivated", in the sense that the interaction between the vapor and the wall is strongly inhibited. The inhibition parameter $K$ is then calibrated in such a way as to prevent spurious condensation without affecting the value of the contact angle at a given values of $G$ and $\Delta$. Remarkably, such calibration procedure proves realizable, in the sense that, with a given $G$, fixing the density ratio, it proves possible to find values of $\Delta$ and $K$ such that the desired value of the contact angle is achieved.

### 3.1 Validation

As a validation test, in Fig. 2, we show the median front position $z(t)$ for the case of two three-dimensional smooth channels, with the following dimensions and contact angles:

- width $W = 1.5\mu$m, height $H = 20\mu$m, length $L = 120\mu$m, $\theta = 54^\circ$;
- width $W = 1.4\mu$m, height $H = 11.4\mu$m, length $L = 140\mu$m, $\theta = 31^\circ$.

For both channels, we set $dx = 0.1\mu$m, corresponding to $15\times200\times1200$ and $14\times114\times1400$ uniform lattices. The main parameters are $G = -5$, $\rho_L = 1.9314$, $\rho_V = 0.156$, $\Delta = 0.2339$, and $K = 0.12$ for $\theta = 54^\circ$, and $\Delta = 0.38$ and $K = 0.12$ for $\theta = 31^\circ$.

These parameters are chosen in such a way to produce essentially the same results as with standard BC on smooth walls, while leaving the functional relation between $\Delta$ and the contact angle, basically intact.

The numerical results are compared against the analytical Washburn solution for a rectangular microchannel [16–18]

$$\widetilde{z}^2 - \widetilde{z}_0^2 = \cos\theta\left(\widetilde{t} - 1 + e^{-\widetilde{t}}\right), \tag{3.2}$$

where $\widetilde{z}$ and $\widetilde{t}$ are dimensionless variables defined as follows:

$$\widetilde{t} = \alpha t, \qquad \widetilde{z} = z\frac{\alpha}{2}\sqrt{\frac{\varepsilon\rho W}{(1+\varepsilon)\sigma}}, \qquad \frac{1}{\alpha} \equiv 8\varepsilon^2\left[1 - \frac{2\varepsilon}{\pi}\tanh\left(\frac{\pi}{2\varepsilon}\right)\right]\pi^{-3}\rho W^2\mu^{-1}.$$

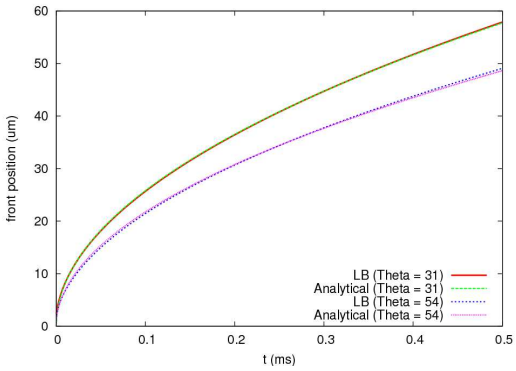


Figure 2: Time evolution of the centerline front position for two different contact angles, $\theta = 31^\circ$ and $\theta = 54^\circ$. LB results versus analytical Washburn solution, Eq. (3.2).

Here $\varepsilon = H/W$ is the aspect ratio of the channel cross section, $\rho$, $\mu$ and $\sigma$ are the fluid density, viscosity and surface tension, respectively. Despite the relatively low density ratio $\rho_L/\rho_V \sim 14$, excellent agreement is observed in both cases.

## 4 Three-dimensional microflows with rugged boundaries

Next, we consider a three-dimensional channel with rough top-bottom boundaries, whose topography is a lattice adaptation of experimental data [19]. The channel dimensions are

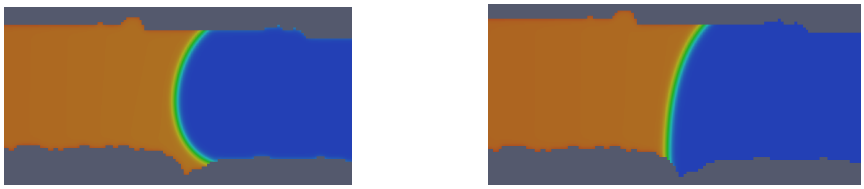

(a) Standard BC at time $t = 147000$ (b) Modified BC at time $t = 147000$

Figure 3: Snapshots of the fluid density at time $t = 147000$. Standard wall boundary conditions (a) and modified (b) are compared. With standard BC, due to condensation in the valley, the front is not slowed-down, while with modified BC the vapor in the valley does not condensate so that the front suffers a temporary slowing-down.

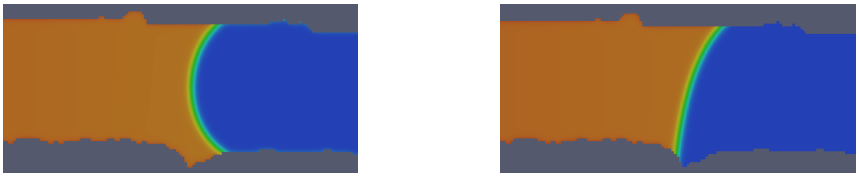

(a) Standard BC at time $t = 154000$ (b) Modified BC at time $t = 154000$

Figure 4: Snapshots of the fluid density at time $t = 154000$. Standard wall boundary conditions (a) and modified (b) are compared. The effect shown in Fig. 3 is further highlighted here, with standard BC, the front moves ahead of the corrugation while with the modified BC, the front slows down and undergoes a (temporary) pinning in the micro-corrugation.

as follows; width $W=3.1\mu$m, height $H=24.5\mu$m (mean height), length $L=413\mu$m. We use a discretization step $dx=0.516\mu$m, corresponding to 48 nodal points across the mainstream direction. A liquid fluid is continuously injected at the inlet with a prescribed density $\rho_L$, corresponding to the equilibrium density of the liquid, while at the outlet a developed flux condition is imposed (zero longitudinal density gradient). The liquid-vapor interface is maintained by a super-critical value of the coupling strength $G=-5$ and a contact angle $\theta=47^\circ$. The values of the liquid and gas densities are set to their equilibrium values, $\rho_L=1.9314$ and $\rho_V=0.156$, respectively (in lattice units).

In Fig. 3, we show a snapshot of the fluid front at time $t=147000$, close to a deep corrugation. From this figure we see that, with standard boundary conditions, due to condensation in the valley, the front goes over the hidden valley with no appreciable slow-down. With the modified boundary conditions, however, the vapor in the valley does not condensate so that, when the front comes to this location, it suffers a temporary slowing-down due to the geometrical corrugation.

This effect is further highlighted in Fig. 4, which show the fluid front at $t=154000$, i.e., 7000 time-steps later. From these figures it is apparent that, with standard BC, the front moves ahead of the corrugation with no additional drag, while with the modified BC, the front slows down and undergoes a (temporary) pinning in the micro-corrugation.

Local condensation effects may produce appreciable changes in the long-term evolution of the front, see Fig. 5. Fig. 5 refers to a microchannel with rough top and bottom walls, the channel dimensions being: Width $W=1.4\mu$m, Height $H=11.4\mu$m (mean height), Length $L=140\mu$m. The walls of the channel are made of PDMS and the fluid injected into the channel is ethanol. The contact angle of ethanol on PDMS is experimentally estimated to be $64^\circ$. The parameter setting for the Shan-Chen model is as above, namely: $G=-5$, $\rho_L=1.9314$ and $\rho_V=0.156$, $\Delta=0.163$, and $K=0.12$, in order to reproduce the experimental contact angle. We use a discretization step $dx=0.1\mu$m, corresponding to a $14\times114\times1400$ lattice. The correlation length of the random profile is $h\sim13$ microns, hence well grid-resolved.

In Fig. 5, we compare the front position as a function of time for both the standard and modified wall boundary condition for this second channel. As one can see, with the standard wall conditions, the front is propagating faster than with the new conditions proposed here. In fact, consistently with two-dimensional findings, it propagates slightly faster than the Washburn solution for a smooth channel of equal dimensions.

Although the correlation length of the random profile is well resolved in the grid, we are nonetheless left with local discrete staircasing effects at the scale of a few lattice sites, hence comparable or smaller than the interface width. Indeed, the r.m.s. of the profile is about 5 lattice spacings, hence quite comparable with the interface width. In order to appraise the sensitivity of the front propagation to grid discreteness, we have repeated the same simulation at a doubled resolution ($dx=0.05\mu$m). The results, shown in Fig. 6, show that indeed, a better resolution of the wall roughness yields an increase of dissipation, thereby resulting in a more marked slowing-down of the front. However, the overall picture remains basically unchanged, with the surface randomness accounting for

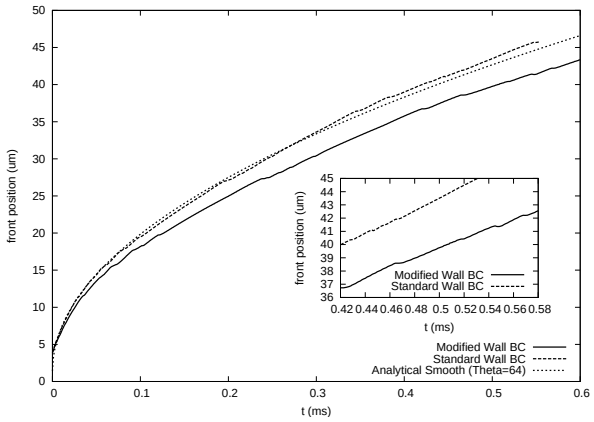


Figure 5: Time evolution of the front with standard and modified boundary condition for the second microchannel, with $W=1.4\mu$m, $H=11.4\mu$m, $L=140\mu$m and contact angle $64^\circ$. Numerical results are also compared with the analytical Washburn profile obtained for $\theta=64^\circ$.

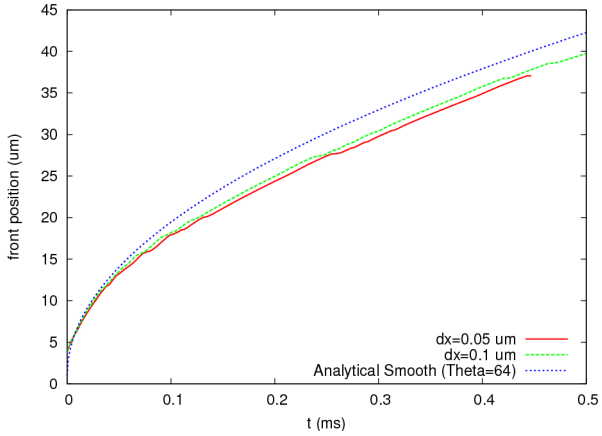


Figure 6: Time evolution of the front with higher resolution $W=1.4\mu$m, $H=11.4\mu$m, $L=70\mu$m and contact angle $64^\circ$. Numerical results are compared with the analytical Washburn profile obtained for $\theta=64^\circ$.

about $5-10\%$ slowing-down over a time span of about 0.5ms. This slowing-down results from the cumulative effects of the sequence of micro-pinning events, the undulations in the trajectory $z(t)$, associated with the local corrugations.

## 5 Conclusions and outlook

In conclusions, we have introduced a new boundary condition aimed at taming spurious condensation effects in lattice Boltzmann simulations of capillary flows in micro-corrugated geometries. In addition, to better resolve the corrugations versus the interface width, high-resolution parallel simulations [20] will be required. The new boundary condition has been validated against the analytical Washburn solution for smooth chan-

nels and demonstrated for the case of three-dimensional capillary microflows over randomly corrugated walls. The simulations indicate an appreciable, although not dramatic, slowing down of the front, due to the surface roughness. For the geometry in point, no hard-pinning events have been detected. The new boundary condition has been postulated on the basis of empirical, yet physically plausible, grounds. In fact, the inhibition parameter $K$ might be associated with some form of chemically heterogeneous coating of the micro-corrugations. Nevertheless, a more systematic theoretical derivation remains to be developed for the future.

## Acknowledgments

Illuminating discussions with G. Parikesit, D. Pisignano, E. Mele and S. Girardo are kindly acknowledged. Financial support through the EC contract NMP3-CT-2006-031980 (INFLUS) is kindly acknowledged.

### References

[1] R. Benzi, S. Succi, and M. Vergassola, The lattice Boltzmann equation: theory and applications, Phys. Rep., 222 (1992), 145–197; D. A. Wolf-Gladrow, Lattice-gas Cellular Automata and Lattice Boltzmann Models, Springer, Berlin, 2000.
[2] S. Succi, Mesoscopic modeling of slip motion at fluid-solid interfaces with heterogeneous catalysis, Phys. Rev. Lett., 89 (2002), 064502.
[3] H. Kusumaatmaja, M. L. Blow, A. Dupuis, and J. M. Yeomans, The collapse transition on superhydrophobic surfaces, Europhys. Lett., 81 (2008), 36003.
[4] J. Hyvaluoma, and J. Harting, Slip flow over structured surfaces with entrapped microbubbles, Phys. Rev. Lett., 100 (2008), 246001.
[5] J. Harting, C. Kunert, and H. J. Herrmann, Lattice Boltzmann simulations of apparent slip in hydrophobic microchannels, Europhys. Lett., 75 (2006), 328–334.
[6] C. Y. Lim, C. Shu, X. D. Niu, and Y. T. Chew, Application of lattice Boltzmann method to simulate microchannel flows, Phys. Fluids., 14 (2002), 2299–2308.
[7] G. Falcucci, S. Ubertini, and S. Succi, Lattice Boltzmann simulations of phase-separating flows at large density ratios: the case of doubly-attractive pseudo-potentials, Soft Matter, 6 (2010), 4357–4365.
[8] P. G. De Gennes, Wetting: statics and dynamics, Rev. Mod. Phys., 57 (1985), 827–863.
[9] E. B. Dussan, On the spreading of liquids on solid surfaces: static and dynamic contact lines, Ann. Rev. Fluid. Mech., 11 (1979), 371–400.
[10] J. Eggers, Hydrodynamic theory of forced dewetting, Phys. Rev. Lett., 93 (2004), 094502.
[11] X. Shan, and H. Chen, Lattice Boltzmann model for simulating flows with multiple phases and components, Phys. Rev. E., 47 (1993), 1815–1819.
[12] M. Sbragaglia, R. Benzi, L. Biferale, S. Succi, and F. Toschi, Surface roughness-hydrophobicity coupling in microchannel and nanochannel flows, Phys. Rev. Lett., 97 (2006), 204503.
[13] C. Cottin-Bizonne, J.-L. Barrat, L. Bocquet, and E. Charlaix, Low-friction flows of liquid at nanopatterned interfaces, Nat. Mater., 2 (2003), 237–240.

[14] F. Diotallevi, L. Biferale, S. Chibbaro, G. Pontrelli, S. Succi, and F. Toschi, Lattice Boltzmann simulations of capillary filling: finite vapour density effects, Europhys. J., 171 (2009), 237–243.
[15] F. Diotallevi, L. Biferale, S. Chibbaro, A. Lamura, G. Pontrelli, M. Sbragaglia, S. Succi, and F. Toschi, Capillary filling using lattice Boltzmann equations: the case of multi-phase flows, Europhys. J., 166 (2009), 111–116.
[16] E. W. Washburn, The dynamics of capillary flow, Phys. Rev., 17 (1921), 273–283.
[17] R. Lucas, Kooloid-Z, 23 (1998), 15.
[18] N. Ichikawa, K. Hosokawa, and R. Maeda, Interface motion of capillary-driven flow in rectangular microchannel, J. Colloid. Interface. Sci., 280 (2004), 155–164.
[19] Courtesy of G. Parikesit.
[20] G. Amati, S. Succi, and R. Piva, Massively parallel lattice Boltzmann simulation of turbulent channel flow, Int. J. Mod. Phys. C, 8 (1997), 869.